Density Functional Study on Formic Acid Decomposition On Pd(111) Surface: A Revisit and Comparison with Other Density Functional Methods

Ni Wang
Changchun Institute of Applied Chemistry Chinese Academy of Sciences: Chang Chun Institute of Applied Chemistry Chinese Academy of Sciences
Kai Li
Changchun Institute of Applied Chemistry Chinese Academy of Sciences: Chang Chun Institute of Applied Chemistry Chinese Academy of Sciences
Ying Wang
Changchun Institute of Applied Chemistry Chinese Academy of Sciences: Chang Chun Institute of Applied Chemistry Chinese Academy of Sciences
Zhijian Wu (zjwu@ciac.ac.cn)
Chang Chun Institute of Applied Chemistry Chinese Academy of Sciences https://orcid.org/0000-0002-8449-8920

Research Article

Keywords: Density functional methods, RPBE, van der Waals interaction, Pd(111), Formic acid.

Posted Date: June 3rd, 2021

DOI: https://doi.org/10.21203/rs.3.rs-567225/v1

Abstract

The mechanism of formic acid decomposition on Pd(111) surface has been investigated by several theoretical methods in previous studies, including PBE and PW91. These results indicated that the mechanism is different from different methods, and even by using the same method (i.e., PBE), the mechanism is also different. In this study, we have revisited the formic acid decomposition on Pd(111) surface by using another density functional RPBE and by including van der Waals interaction which is neglected in the previous studies. Our results showed that the formic acid is decomposed via O-H bond cleavage to form bi-HCOO*, and the most favorable pathway is HCOOH* → bi-HCOO*+H* → CO_2+2H*. The energy barrier is 0.55 eV at the rate-determining step. This conclusion is consistent with one of the PBE study. This demonstrated that computational methods have great influence on the reaction mechanism, and care should be taken in selecting the appropriate computational methods.

1. Introduction

Energy crisis has become one of the biggest challenges for human society due to the rising energy demands. To solve the problem, fuel cells are studied extensively because they can convert the chemical energy of fuels into electrical energy directly to alleviate the energy shortage [1]. To date, the direct formic acid fuel cell (DFAFC) has attracted great attention as potential power source due to its advantages such as safety, high electrode potential, lower crossover current, and appropriate power densities at low temperatures [2-5].

Nowadays, Pd and Pd-based catalysts are commonly employed for the dissociation of formic acid in DFAFCs [6]. Pd is considered as the most active catalyst among the pure metals. There are two possible pathways for formic acid (FA) decomposition on the Pd(111) surface, i.e., the dehydrogenation pathway (HCOOH → CO_2+H_2) and the dehydration pathway (HCOOH → CO+H_2O). The dehydration pathway would not only decrease the production of hydrogen, but also produce the adsorbed CO to degrade the catalytic performance of Pd [7]. Thus, the method of improving the selectivity of FA decomposition (via dehydrogenation pathway) is desirable. To achieve this goal, FA decomposition on Pd surface has been studied both experimentally [8-12] and theoretically [13-18]. The experimental study showed that the reaction pathway on Pd(111) surface proceeds primarily via a dehydrogenation pathway at 280 K with the formation of CO_2 and H_2, and $HCOO^-$ generated by the cleavage of O-H bond in HCOOH is an important intermediate to enhance the reaction rate [8]. It has also been observed that on Pd(111) surface, $HCOO^-$ is much more efficiently decomposed than HCOOH and the C-H bond cleavage is found to be the rate-determining step on Pd/C catalyst [11]. By including NH_3 on the Pd(111) surface, CO species is inhibited and the FA decomposition mainly goes through the dehydrogenation pathway [12]. Besides pure Pd catalyst, there are also many studies focus on the Pd based alloys, such as Pd-Au [19], Pd-Ag [20], and Pd alloying with other metals [21-23] in order to enhance the dehydrogenation pathway. For the theoretical study, it is reported that the dehydrogenation pathway of FA decomposition on Pd(111) surface is the dominate pathway [14,17] based on the different density functionals. However, the

obtained rate determining step is found to be different. By using PW91 [24], it has been found that the rate-determining step is the cleavage of O-H bond of HCOOH* to generate HCOO* with the energy barrier of 1.00 eV [14]. By using PBE [25], the cleavage of C-H bond of bidentate HCOO* to form CO_2+H_2 is the rate-determining step with the energy barrier of 0.79 eV [17]. In addition, a study based on PBE showed that by locating two new configurations for HCOOH adsorption on Pd(111), the formation of CO is predicted to be competing with the formation of CO_2 [15].

Motivated by the above study, in this work, we have revisited the FA dissociation on Pd(111) surface by using the revised Perdew–Burke-Ernzerhof functional (RPBE) [26] and including van der Waals (vdW) interaction. RPBE is known to be more accurate in describing the adsorption energy of the reaction intermediate on the catalyst surface [26], compared with PBE and PW91 functionals. In addition, the impact of vdW correction was demonstrated to be important for FA dissociation on transition metal surface and agreement with experimental study is achieved by including the vdW interaction [27].

2. Computational Details

2.1 Method

All calculations were carried out using Vienna ab-initio simulation package (VASP) [28-31]. The interaction between ion cores and valence electrons were described by the projector augmented wave (PAW) method [32]. The revised Perdew–Burke-Ernzerhof (RPBE) functional [26] was adopted to describe the exchange and correlation effects. The wave functions at each k-point were expanded with a plane wave basis set. The kinetic cutoff is set to be 400 eV. The Brillouin zone was sampled by a 3 3 1 Monkhorst Pack k-point mesh [33], while the Fermi surface was treated with second-order Methfessel–Paxton smearing [34] with a width of 0.1 eV to accelerate electronic convergence. The geometries were optimized until the energy was converged to 1.0 10^{-5} eV/atom and the force to 0.05 eV/Å. Spin polarization was considered during all calculations. The van der Waals (vdW) interaction calculated with D2 was considered throughout the study. The climbing image nudged elastic band (CI-NEB) method was adopted to find a minimum energy pathway and the transition state (TS) structures [35]. The minimum energy pathway was optimized using a force-based conjugate-gradient method [31] until the maximum force was less than 0.05 eV/Å.

2.2 Model

The most stable face-center-cubic (111) surface of close-packed Pd metal is modeled using a four atomic layers p(33) supercell to investigate the catalytic mechanism of FA decomposition. A vacuum layer of 12 Å along the z direction is set to separate the periodically repeated slabs. For the Pd(111) surface, the bottom two layers were fixed, while the upper two layers were relaxed during the geometry optimization. The structure of clean Pd(111) surface are shown in Fig.1 with possible adsorption sites. The adsorption

energies are defined as $\Delta E_{ads} = E_{total} - E_{surface} - E_{adsorbate}$, where $E_{adsorbate}$, E_{surf}, and E_{total} are the energies of free adsorbate, the clean surface, and the adsorbed system, respectively.

3. Results And Discussion

3.1 Geometries and adsorption of species in FA decomposition

For the possible species in FA decomposition, the obtained most stable configurations are presented in Fig. 2. The corresponding adsorption energies and selected bond distances are listed in Table 1.

HCOOH. The reaction of FA decomposition starts with the adsorption of gaseous HCOOH. After it is adsorbed on the Pd surface, two different isomers have been obtained, i.e., trans-HCOOH* and cis-HCOOH* (Fig. 2). For trans-HCOOH*, the H atom in hydroxyl group (OH) points toward the bridge site on the Pd surface and trans-HCOOH* bonds with Pd atom at the top site by another O atom with the Pd-O bond distance of 2.33 Å, in agreement with the previous study [17]. For cis-HCOOH*, it also bonds with Pd atom at the tope site with the Pd-O bond distance of 2.58 Å, but the H atom in OH pointing away from the catalyst surface. The adsorption energy for trans-HCOOH* is -0.71 eV (Table 1), stronger than -0.62 eV by PW91 [14] and -0.37 eV by PBE [17]. This could be caused by the different theoretical methods or the vdW interaction considered in this work, or both. For cis-HCOOH*, the adsorption energy is weak (-0.34 eV) compared with the trans-HCOOH*. This value (-0.34 eV) is stronger than -0.11 eV by PBE [17], but weaker than -0.41 eV by PW91 [14]. In addition, the parallel adsorption structure of HCOOH* with Pd surface in the previous study [15, 36] has also been taken into account, in which HCOOH* bonds with the surface through C, O atoms. But unfortunately, we failed to locate this structure.

Table 1 Adsorption sites, bond distances (Å) and adsorption energies (eV) for the most stable adsorbed species in formic acid decomposition on the Pd(111) surface. Comparison is made with the previous studies.

	RPBE				PBE [a]		PW91 [b]	
	site	ΔE_{ads}	$d_{Pd-C/H}$	d_{Pd-O}	site	ΔE_{ads}	site	ΔE_{ads}
trans-HCOOH	top	-0.71		2.33	top	-0.37	top	-0.62
cis-HCOOH	top	-0.34		2.58	top	-0.11	top	-0.41
bi-HCOO	bri	-2.58		2.17, 2.17	bri	-2.32	bri	-2.70
mono-HCOO	top	-1.92	1.97	2.10	top	-1.54	top	-2.04
trans-COOH	top	-2.55	2.00		bri	-2.16	top	-2.57
cis-COOH	top	-2.38	1.99		bri	-2.15	top	-2.41
CO_2	bri	-0.19		3.22,3.22	bri	-0.02	bri	-0.18
CO	fcc	-2.00	2.02, 2.06, 2.08		fcc	-2.04	fcc	-2.05
H	fcc	-2.82	1.81		fcc	-2.87	fcc	-2.91
OH	bri	-2.44		2.15 ,2.17	bri	-2.57	bri	-2.62
H_2O	top	-0.31		2.51	top	-0.25	top	-0.51

[a] Ref. [17] and [b] Ref. [14]

HCOO. HCOO* is the main intermediate in FA decomposition. It bonds with the Pd surface and forms two isomers, i.e., bi-dentate HCOO* (bi-HCOO*) and mono-dentate HCOO* (mono-HCOO*). For bi-HCOO*, both O atoms bonds with Pd surface with the same bond distance of 2.17 Å (Fig. 2 and Table 1). The adsorption energy is -2.58 eV, indicating a very strong adsorption. For mono-HCOO*, only the O atom at the carbonyl group (C=O) bonds with the Pd atom with Pd-O bond distance of 2.10 Å. Meanwhile, the H atom in C-H bond of mono-HCOO* points toward the atop Pd atom with a distance of 1.97 Å. The adsorption energy is -1.92 eV, much weaker than -2.58 eV for bi-HCOO*, consistent with the previous studies [14,17].

COOH. Similar to HCOO*, there are also two isomers for COOH*, i.e., trans-COOH* and cis-COOH*. For both configurations, only C atom bonds with Pd surface with the bond distances of 2.00 Å for trans-COOH* and 1.99 Å for cis-COOH*. For trans-COOH*, the H atom points away from the Pd surface with the adsorption energy of -2.55 eV. For cis-COOH*, the H atom points toward the Pd surface with the adsorption energy of -2.38 eV, weaker than trans-COOH*. From Table 1, we also noted that in this study and previous study by PW91 [14], both COOH* isomers adsorbed on the Pd top site, while they are adsorbed at the bridge site from the PBE study with nearly the same adsorption energies [17].

CO_2. For adsorbed CO_2, O-C-O bond angle is 179.3°, slightly deviated from the linear structure. The C=O bond distance is 1.18 Å, nearly the same as in the gaseous CO_2 molecule, suggesting that CO_2 is

adsorbed physically on the surface. The adsorption energy is -0.19 eV, similar to -0.18 eV by PW91 [14], but stronger than -0.02 eV by PBE study [17].

CO. CO* is adsorbed on the fcc site with three slightly different Pd-C bond distances (Table 1). This is consistent with the experimental observation that CO* occupied hollow site by scanning tunneling microscopy [37]. The adsorption energy is -2.00 eV, similar to -2.05 eV by PW91 [14] and -2.04 eV by PBE [17].

H. H* atom can be stably adsorbed at the fcc site on Pd surface. This is in agreement with the experimental observation by low-energy electron diffraction that H* atom resides at fcc 3-fold hollow site on Pd(111) surface [38]. The calculated adsorption energy is -2.82 eV, also close to experimental value of -2.68 eV [39].

OH. For OH*, it prefers to bind at the bridge site with the adsorption energy of -2.44 eV. The two Pd-O bond distances are slightly different, i.e., 2.15 Å and 2.17 Å, respectively.

H_2O. H_2O interacts weakly with the Pd surface with the Pd-O distance of 2.51 Å. The adsorption energy is -0.31 eV, weaker than -0.51 eV by PW91 [14], but slightly stronger than -0.25 eV by PBE [17].

By comparing different methods, we noted that the adsorption energies from RPBE in this study lie between PBE and PW91 for cis-HCOOH*, bi-HCOO*, mono-HCOO*, trans-COOH*, cis-COOH* and H_2O (Table 1). For trans-HCOOH* and CO_2, the adsorption energies from RPBE are the strongest, while for CO*, H*, and OH*, RPBE gives the weakest adsorption energies.

3.2 FA decomposition mechanism

After obtaining the most stable adsorption structures, we can now procced to study the FA decomposition mechanism. The corresponding results are shown in Fig. 3 and Fig. 4. For comparison, our results are also presented in Scheme 1 together with previous theoretical studies.

FA decomposition via O-H bond cleavage (Fig. 3). In this mechanism, the first step is the FA dehydrogenation via O-H bond cleavage to form bi-HCOO*. In this step, the O-H bond in HCOOH* is elongated from the initial distance of 1.02 Å to 1.78 Å in transition state TS1. The energy barrier is 0.55 eV with slightly endothermic by 0.07 eV. We know that for isolated bi-HCOO* on the Pd surface, both Pd-O bond distances are the same (Table 1). However, for the complex state bi-HCOO* + H*, the existence of H atom makes the two Pd-O bonds having different distances, i.e., 2.16 and 2.23 Å, respectively. Subsequently, the longer Pd-O bond (2.23 Å) would be broken and the HCOO* species is rotated to form mono-HCOO*, in which the H atom in C-H group points toward Pd surface, which would be beneficial for C-H breaking. The reaction energy barrier in this step is 0.73 eV, which is also the rate-determining step. After the formation of mono-HCOO*, the formation of final product of CO_2+2H* is very easy due to the negligible energy barrier of 0.06 eV. Thus, for the pathway trans-HCOOH* → bi-HCOO*+H* → mono-

HCOO*+H* → CO_2+2H*, the rate determining step is from bi-HCOO* to mono-HCOO*, similar to the previous study by PBE [15,17] (see also Scheme 1). For the other pathway, i.e., trans-HCOOH* → bi-HCOO*+H* → CO_2+2H*, CO_2 is produced directly from bi-HCOO*. In this pathway, the direct decomposition of bi-HCOO* is carried out through the cleavage of the longer Pd-O bond and the torsional deformation to form TS4, in which H atom in C-H is close to Pd surface. The energy barrier is 0.55 eV and the reaction is exothermic by -0.69 eV. This means that in the pathway trans-HCOOH* → bi-HCOO*+H* → CO_2+2H*, both steps have the same energy barrier of 0.55 eV and are the rate-determining steps. This indicated that for the FA decomposition via O-H bond cleavage, pathway trans-HCOOH* → bi-HCOO*+H* → CO_2+2H* is preferred. This is in agreement with the previous study by PBE [17].

FA decomposition via C-H bond cleavage (Fig. 4). The C-H bond cleavage in trans-HCOOH* would produce the intermediate trans-COOH*. The energy barrier is 0.68 eV. After trans-COOH* is formed, there are three possible pathways to produce the final products, i.e., trans-COOH*+H* → CO_2+2H*, trans-COOH*+H* → CO*+H_2O, and trans-COOH*+H* → cis-COOH*+H* → CO*+H_2O (Fig. 4). For trans-COOH* directly converts to CO_2+2H*, the energy barrier is 1.11 eV and exothermic by -0.50 eV. For trans-COOH* converts to CO*+H_2O, the energy barrier is similar, i.e., 1.18 eV. This suggested that the direct conversion of trans-COOH* to the final product is difficult due to the high energy barriers. In contrast, the pathway trans-COOH*+H* → cis-COOH*+H* → CO*+H_2O has relatively low energy barriers. The energy barrier is 0.51 eV from trans-COOH* to cis-COOH*, 0.64 eV from cis-COOH*+H* to CO*+H_2O, which is more favorable. Thus, for FA decomposition via C-H bond cleavage, pathway trans-HCOOH* → trans-COOH*+H* → cis-COOH*+H* → CO*+H_2O is favorable. The rate determining step is the formation of trans-COOH* from trans-HCOOH* with the energy barrier of 0.68 eV, in agreement with the previous study by PBE [17].

In a word, the above study showed that the FA decomposition via O-H bond cleavage is favored with the pathway of trans-HCOOH* → bi-HCOO*+H* → CO_2+2H*. The energy barrier is 0.55 eV at the rate determining step, lower than 0.68 eV in the pathway of trans-HCOOH*→ trans-COOH*+H* → cis-COOH*+H* → CO*+H_2O for CO production (Scheme 1). This conclusion is in agreement with the previous study by PBE [17], but different from the study by PW91 [14], in which the most favorable pathway is trans-HCOOH* → bi-HCOO*+H* → mono-HCOO*+H* → CO_2+2H* (Scheme 1). Meanwhile, we also noted that in another study by PBE [15], the most favorable pathway is trans-HCOOH* → cis-COOH*+H* → CO*+H_2O, while the most favorable pathway in this work, i.e., trans-HCOOH* → bi-HCOO*+H* → CO_2+2H*, is not examined in Ref. 15. This demonstrated that computational methods would have great influence on both the geometries and electronic properties, and care should be taken in choosing the computational methods, for instance, calibrating the theoretical methods by comparing with the experimental study or more reliable theoretical methods. In addition, since the same method gives different conclusions, this remind us that we should be very careful in selecting the initial and final structures during the reaction.

Finally, from Scheme 1, we have also found something in common. All these theoretical studies showed that the formation of bi-HCOO* from HCOOH* is more favorable compared to the formation of trans-

COOH* (HCOOH* → bi-HCOO* vs HCOOH* → trans-COOH*). Dehydrogenation pathway is favored along bi-HCOO* pathway, while dehydration pathway prefers to follow trans-COOH*. The formation of CO_2+2H* from mono-HCOO (mono-HCOO* → CO_2+2H*) is very easy due to the negligible energy barrier. This implies that mono-HCOO* can not exist stably on the catalyst surface because it will be dissociated immediately to the final product once it is formed. For the formation of CO*+H_2O, the main intermediate is cis-COOH* and trans-COOH* is relatively easy to be transformed to cis-COOH*, while direct formation of CO*+H_2O from trans-COOH* is difficult. This means that if more HCOO* species can be obtained experimentally and meanwhile reduce the formation of COOH*, the production yield of hydrogen would be high.

4. Conclusions

The formic acid decomposition on Pd(111) surface is revisited by using the density functional RPBE and by including the van der Waals interaction. Our calculations showed that FA decomposition is through the O-H bond cleavage pathway, and the most favorable pathway is HCOOH* → bi-HCOO*+H* → CO_2+2H*. The energy barrier is 0.55 eV at the rate determining step, lower than 0.68 eV in the pathway for CO production. This means that the dehydrogenation pathway is preferred over dehydration pathway. This conclusion is in agreement with one of the previous PBE study [17]. Meanwhile, the inconsistent conclusions from the previous theoretical studies based on different methods remind us that we should be careful in selecting both the theoretical methods and the initial and final structures during the reaction.

Declarations

Acknowledgements

This work is supported by the National Natural Science Foundation of China (21733004, 21673220) and the National Key Research and Development Program of China (2016YFA0602900). The computational time is supported by the High Performance computing center of Jilin University, computing center of Jilin Province and computing center of Changchun Institute of Applied Chemistry.

Funding

The work is supported by the National Natural Science Foundation of China (21733004, 21673220) and the National Key Research and Development Program of China (2016YFA0602900).

Conflict of interest

The authors declare no competing interests.

Author information

Wang Ni

Chang Chun Institute of Applied Chemistry Chinese Academy of Sciences

Li Kai

Chang Chun Institute of Applied Chemistry Chinese Academy of Sciences

Wang Ying

Chang Chun Institute of Applied Chemistry Chinese Academy of Sciences

Wu Zhijian

Chang Chun Institute of Applied Chemistry Chinese Academy of Sciences

Availability of data and material: (data transparency)

All data generated or analysed during this study are included in this published article.

Code availability: (software application or custom code)

VASP software package.

Authors' contributions

Wang Ni wrote the paper and contributed to the acquisition, drafting, analysis, working, and interpretation of data. Li Kai and Wang Ying had substantial contribution to the research design, the acquisition, analysis, and interpretation of data. Wu Zhijian had contributed to the analysis, interpretation of data, and paper writing ideas, making significant contributions to submitted and final manuscript revisions.

References

1. Aricò A, Bruce P, Scrosati B, Tarascon JM, Schalkwijk WV (2005) Nanostructured materials for advanced energy conversion and storage devices. Nat. Mater. 4:366-377. https://doi.org/10.1038/nmat1368.
2. Johnson TC, Morris DJ, Wills M (2010) Hydrogen generation from formic acid and alcohols using homogeneous catalysts. Chem. Soc. Rev. 39:81-88. http://dx.doi.org/10.1039/B904495G.
3. Rice C, Ha S, Masel RI, Waszczuk P, Wieckowski A, Barnard T (2002) Direct formic acid fuel cells. J. Power Sources 111:83-89. https://doi.org/10.1016/S0378-7753(02)00271-9.
4. Wang X, Hu JM, Hsing IM (2004) Electrochemical investigation of formic acid electro-oxidation and its crossover through a Nafion membrane. J. Eletroanal. Chem. 562:73-80. https://doi.org/10.1016/j.jelechem.2003.08.010.
5. Zhu Y, Ha SY, Masel RI (2004) High power density direct formic acid fuel cells. J. Power Sources 130:8-14. https://doi.org/10.1016/j.jpowsour.2003.11.051.

6. Yu XW, Pickup PG (2008) Recent advances in direct formic acid fuel cell (DFAFC). J. Power Sources 182:124-132. https://doi.org/10.1016/j.jpowsour.2008.03.075.
7. Ozensoy E, Min BK, Santra AK, Goodman DW (2004) CO dissociation at elevated pressures on supported Pd nanoclusters. J. Phys. Chem. B 108:4351-4357. https://doi.org/10.1021/jp030928o.
8. Davis JL, Barteau MA (1991) Reactions of carboxylic acids on the Pd(111)-(2×2)O surface: Multiple roles of surface oxygen atoms. Surf. Sci. 256:50-66. https://doi.org/10.1016/0039-6028(91)91199-8.
9. Patra S, Viswanath B, Barai K, Ravishankar N, Munichandraiah N (2010) High-surface step density on dendritic Pd leads to exceptional catalytic activity for formic acid oxidation. ACS Appl. Mater. Interfaces 2:2965-2969. https://doi.org/10.1021/am100647u.
10. Mori K, Dojo M, Yamashita H (2013) Pd and Pd-Ag nanoparticles within a macroreticular basic resin: An efficient catalyst for hydrogen production from formic acid decomposition. ACS Catal. 3:1114-1119. https://doi.org/10.1021/cs400148n.
11. Lv Q, Meng Q, Liu W, Sun N, Jiang K, Ma L et al. (2018) Pd–PdO interface as active site for HCOOH selective dehydrogenation at ambient condition. J. Phys. Chem. C 122:2081-2088. https://doi.org/10.1021/acs.jpcc.7b08105.
12. Karakurt B, Kocak Y, Ozensoy E (2019) Enhancement of formic acid dehydrogenation selectivity of Pd(111) single crystal model catalyst surface via Brønsted bases. J. Phys. Chem. C 123:28777-28788. https://doi.org/10.1021/acs.jpcc.9b08707.
13. Luo Q, Feng G, Beller M, Jiao H (2012) Formic acid dehydrogenation on Ni(111) and comparison with Pd(111) and Pt(111). J. Phys. Chem. C 116:4149-4156. https://doi.org/10.1021/jp209998r.
14. Zhang R, Liu H, Wang B, Ling L (2012) Insights into the preference of CO_2 formation from HCOOH decomposition on Pd surface: A theoretical study. J. Phys. J. Phys. Chem. C 116:22266-22280. https://doi.org/10.1021/jp211900z.
15. Wang Y, Qi Y, Zhang D, Liu C (2014) New insight into the decomposition mechanism of formic acid on Pd(111): Competing formation of CO_2 and CO. J. Phys. Chem. C 118:2067-2076. https://doi.org/10.1021/jp410742p.
16. Herron JA, Scaranto J, Ferrin P, Li S, Mavrikakis M (2014) Trends in formic acid decomposition on model transition metal surfaces: A density functional theory study. ACS Catal. 4:4434-4445. https://doi.org/10.1021/cs500737p.
17. He F, Li K, Xie G, Wang Y, Jiao M, Tang H, Wu ZJ (2016) Understanding the enhanced catalytic activity of Cu_1@Pd_3(111) in formic acid dissociation, a theoretical perspective. J. Power Sources 316:8-16. https://doi.org/10.1016/j.jpowsour.2016.03.062.
18. Chen BWJ, Mavirkakis M (2020) Formic acid: A hydrogen-bonding cocatalyst for formate decomposition. ACS Catal. 10:10812-10825. http://dx.doi.org/10.1021/acscatal.0c02902.
19. Yang L, Li G, Chang J, Ge J, Liu C, Vladdimir F, Wang G, Jin Z, XingW (2020) Sea urchin-like Aucore@Pdshell electrocatalysts with high FAOR performance: Coefficient of lattice strain and

electrochemical surface area. Appl. Catal. B 260:118200. https://doi.org/10.1016/j.apcatb.2019.118200.

20. Tedsree K, Li T, Jones S, Chan CWA, Yu KMK, Bagot PAJ et al. (2011)Hydrogen production from formic acid decomposition at room temperature using an Ag-Pd core-shell nanocatalyst. Nat. Nanotechnol. 6:302-307. https://doi.org/10.1038/nnano.2011.42.
21. Yang M, Wang B, Li Z, Ling L, Zhang R (2020) HCOOH dissociation over the core-shell M@Pd bimetallic catalysts: Probe into the effect of the core metal type on the catalytic performance. Appl. Surf. Sci. 506:114938. https://doi.org/10.1016/j.apsusc.2019.144938.
22. Cho J, Lee S, Yoon SP, Han J, Nam SW, Lee KY, Ham HC (2017) Role of heteronuclear interactions in selective H_2 formation from HCOOH decomposition on bimetallic Pd/M (M = Late Transition FCC Metal) catalysts. ACS Catal. 7:2553-2562. https://doi.org/10.1021/acscatal.6b02825.
23. Jiang K, Xu K, Zou S, Cai WB (2014) B-doped Pd catalyst: Boosting room-temperature hydrogen production from formic acid-formate solutions. J. Am. Chem. Soc. J. Am. Chem. Soc. 136:4861-4864. https://doi.org/10.1021/ja5008917.
24. Perdew JP, Wang Y (1992) Accurate and simple analytic representation of the electron-gas correlation energy. Phys. Rev. B 45:13244-13249. https://doi.org/10.1103/PhysRevB.45.13244.
25. Perdew JP, Burke K, Ernzerhof M (1996) Generalized gradient approximation made simple. Phys. Rev. Lett. 77:3865. https://doi.org/10.1103/PhysRevLett.77.3865.
26. Hammer B, Hansen LB, Nørskov JK (1999) Improved adsorption energetics within density-functional theory using revised Perdew-Burke-Ernzerhof functionals. Phys. Rev. B 59:7413-7420. https://doi.org/10.1103/PhysRevB.59.7413.
27. Yoo JS, Abild-Pedersen F, Nørskov JK, Studt F (2014) Theoretical analysis of transition-metal catalysts for formic acid decomposition. ACS Catal. 4:1226-1233. https://doi.org/10.1021/cs400664z.
28. Kresse G, Furthmüller J (1996) Efficiency of ab-initio total energy calculations for metals and semiconductors using a plane-wave basis set. Comp. Mater. Sci. 6:15-50. https://doi.org/10.1016/0927-0256(96)00008-0.
29. Kresse G, Hafner (1993) Ab initio molecular dynamics for liquid metals. J Phys. Rev. B 47:558. https://doi.org/10.1103/PhysRevB.47.558.
30. Kresse G, Hafner (1994) Ab initio molecular-dynamics simulation of the liquid-metal-amorphous-semiconductor transition in germanium. J Phys. Rev. B 49:14251. https://doi.org/10.1103/PhysRevB.49.14251.
31. Kresse G, Furthmüller J (1996) Efficient iterative schemes for ab initio total-energy calculations using a plane-wave basis set. Phys. Rev. B 54:11169. https://doi.org/10.1103/PhysRevB.54.11169.
32. Blöchl PE, Kästner J, Först CJ (1994) Projector augmented-wave method. Phys. Rev. B 50:17953. https://doi.org/10.1103/PhysRevB.50.17953.

33. Monkhorst HJ, Pack JD (1976) Special points for Brillouin-zone integrations. Phys. Rev. B 13:5188-5192. https://doi.org/10.1103/PhysRevB.13.5188.
34. Methfessel M, Paxton AT (1989) High-precision sampling for Brillouin-zone integration in metals. Phys. Rev. B 40:3616. https://doi.org/10.1103/PhysRevB.40.3616.
35. Henkelman G, Uberuaga BP, Jónsson H (2000) A climbing image nudged elastic band method for finding saddle points and minimum energy paths. J. Chem. Phys. 113:9901-9904. https://doi.org/10.1063/1.1329672.
36. Zhou SD, Qian C, Chen XZ (2011) Comparative theoretical study of adsorption and dehydrogenation of formic acid, hydrazine and isopropanol on Pd(111) surface. Catal. Lett. 141:726-734. https://doi.org/10.1007/s10562-011-0553-y.
37. Sautet P, Rose MK, Dunphy JC, Behler S, Salmeron M (2000) Adsorption and energetics of isolated CO molecules on Pd(111). Surf. Sci. 453:25-31. https://doi.org/10.1016/S0039-6028(00)00243-0.
38. Felter TE, Sowa EC (1989) Location of hydrogen adsorbed on palladium (111) studied by low-energy electron diffraction. Phys. Rev. B 40:891. https://doi.org/10.1103/PhysRevB.40.891.
39. Shustorovich E (1990) The bond-order conservation approach to chemisorption and heterogeneous catalysis: Applications and implication. Adv. Catal. 37:101-163. https://doi.org/10.1016/S0360-0564(08)60364-8.

Figures

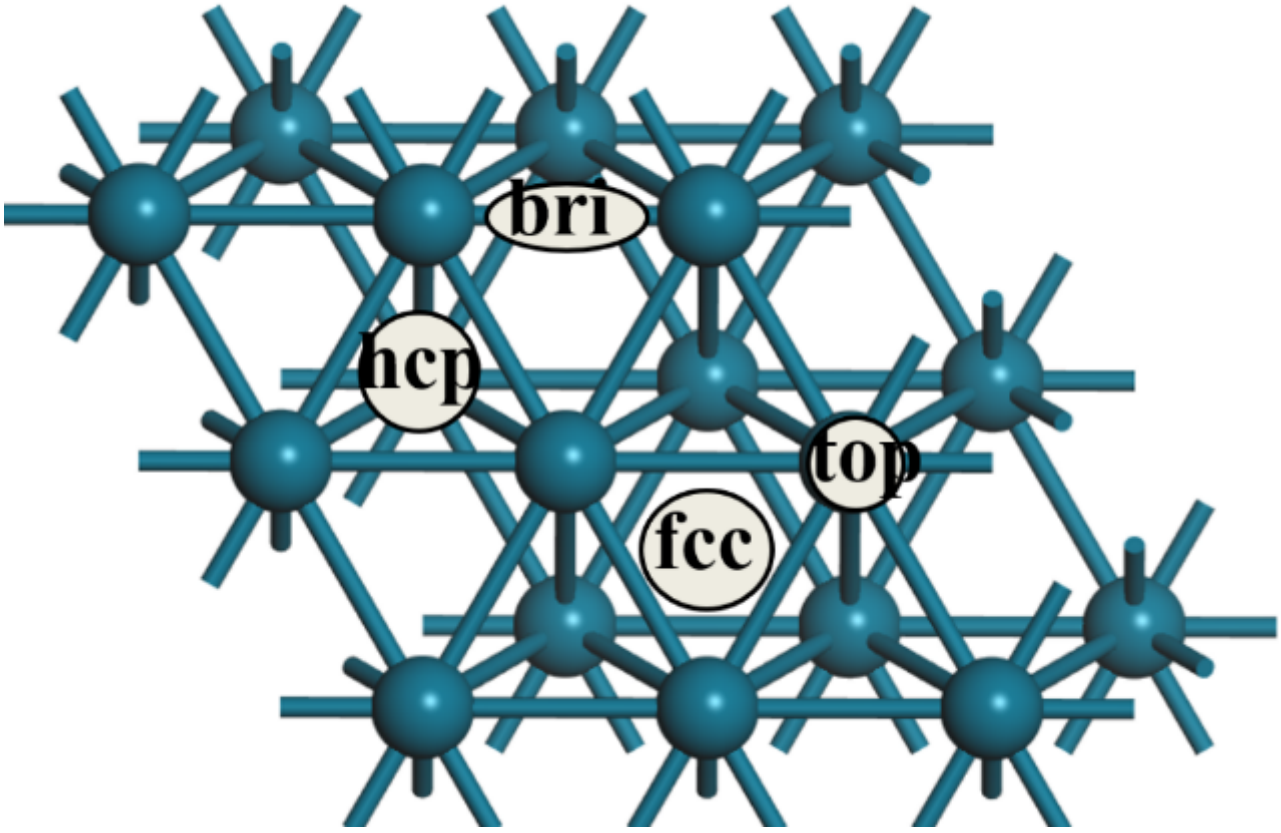

Figure 1

Top view of the Pd(111) surface and possible adsorbed sites, i.e., top site, bridge site, hexagonal-close packed site (hcp), and face-centered-cubic site (fcc). For clarity, only two layers are displayed.

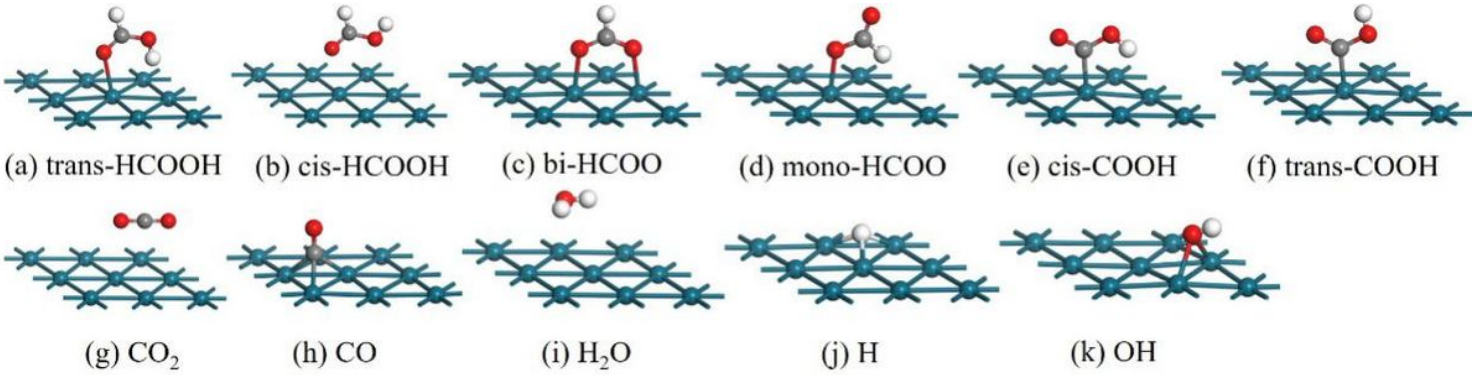

Figure 2

The most stable adsorption configurations for the species during the formic acid decomposition on Pd(111) surface. The red, gray, white and dark-blue balls are O, C, H and Pd atoms, respectively.

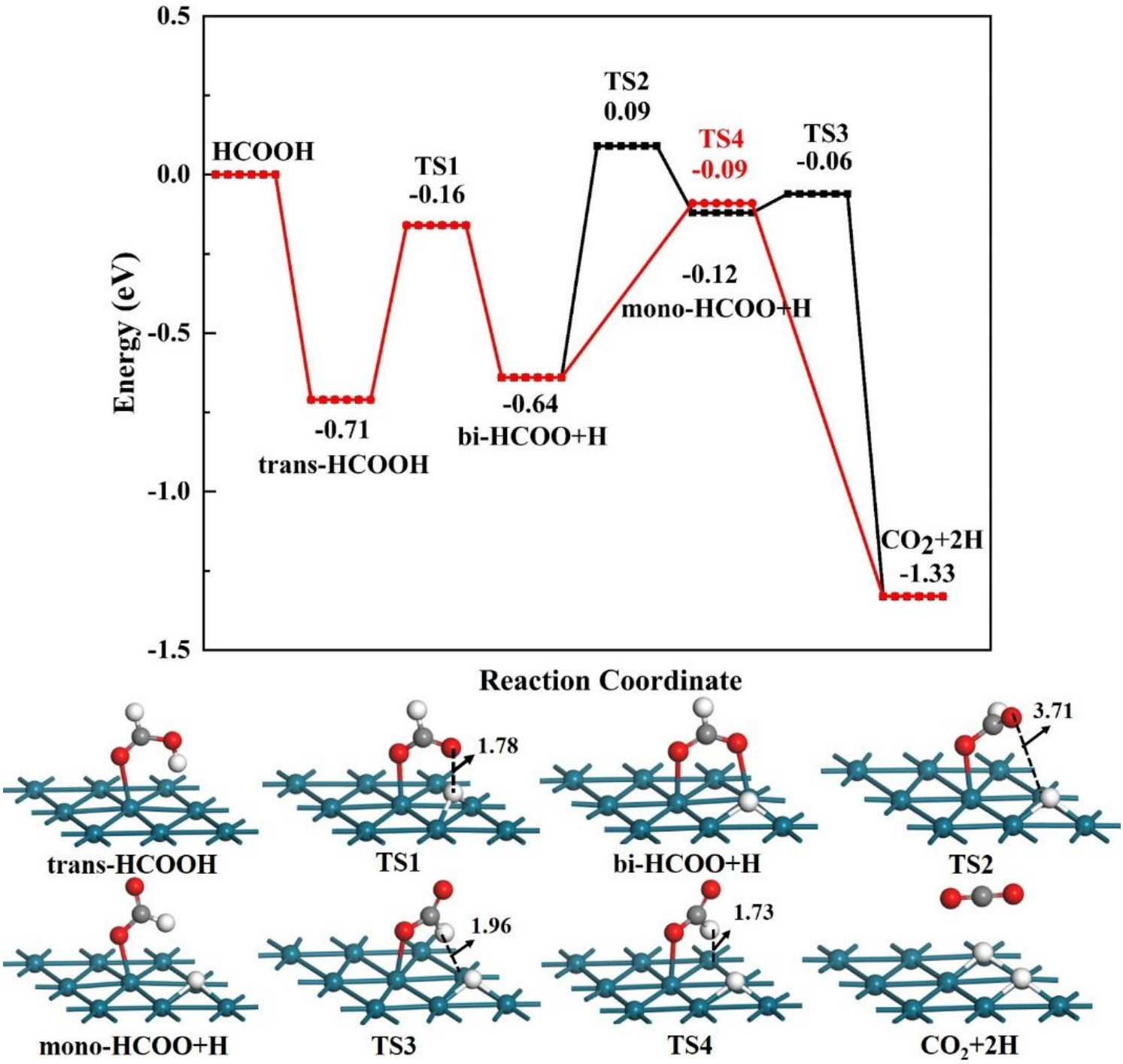

Figure 3

Potential energy profiles for trans-HCOOH decompose through O-H bond cleavage.

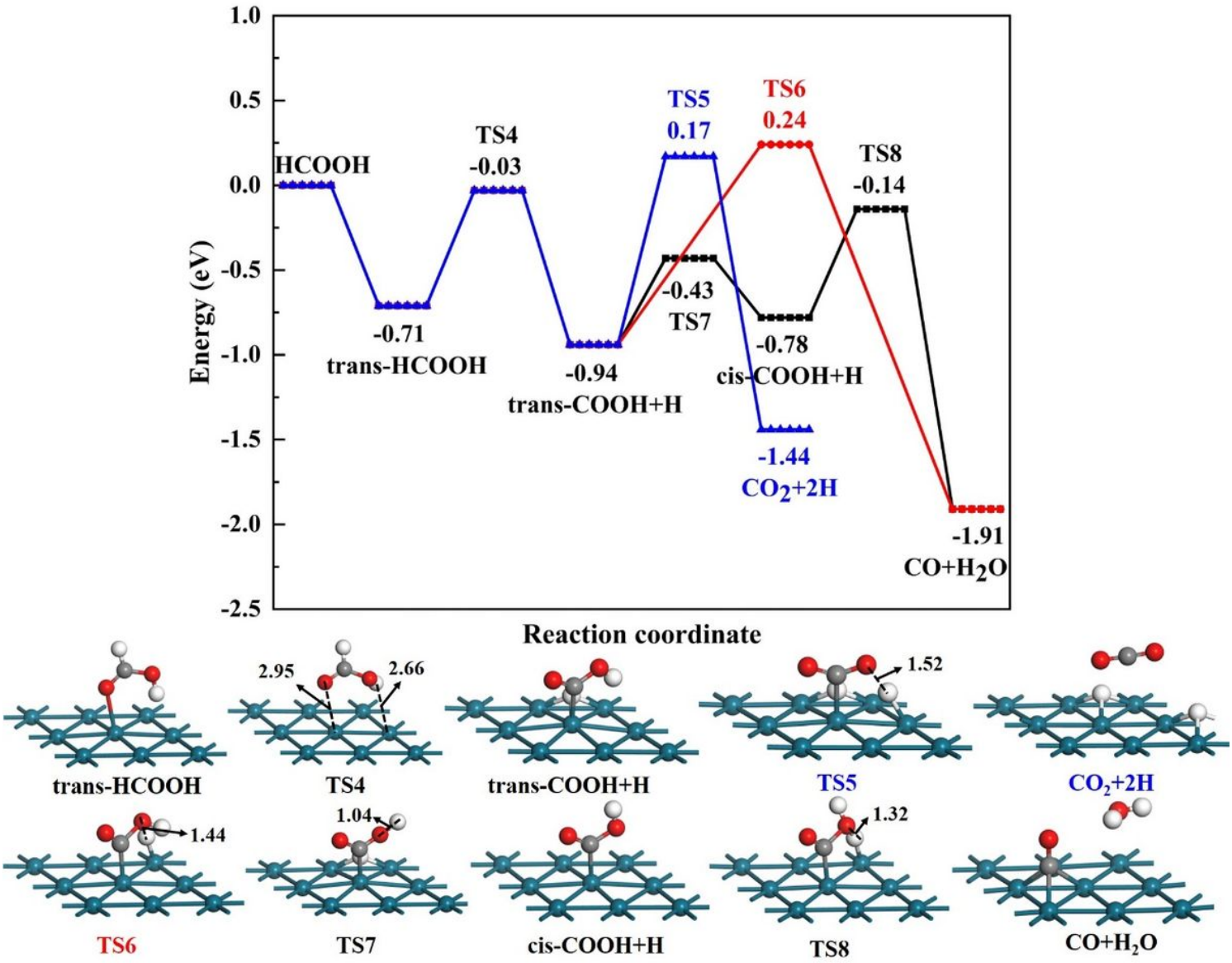

Figure 4

Potential energy profiles for trans-HCOOH decomposition initiated by C-H bond cleavage.

Supplementary Files

This is a list of supplementary files associated with this preprint. Click to download.

- floatimage5.jpeg